

Low-temperature ground state structure of PbTiO_3

V. Laguta^{1,2}, Yu. O. Zagorodniy², R. O. Kuzian^{2,3}, I. V. Kondakova², V. Chlan⁴, R. Řezníček⁴,
H. Štěpánková⁴, D. Bohdanov¹, J. Hlinka¹ and R. Ramesh⁵


¹*Institute of Physics, Academy of Sciences of the Czech Republic, 18200 Prague, Czech Republic*

²*Institute for Problems of Materials Science NAS Ukraine, 03142 Kyiv, Ukraine*

³*Donostia International Physics Center (DIPC), 20018 Donostia/San Sebastian, Basque Country, Spain*

⁴*Charles University, Faculty of Mathematics and Physics, 18000 Prague, Czech Republic*

⁵*University of California, Department of Materials Science and Engineering and Department of Physics, Berkeley, California 94720, USA*

 (Received 22 December 2022; revised 6 March 2023; accepted 16 March 2023; published 28 March 2023)

Mn^{4+} , Cr^{3+} , and Fe^{3+} electron paramagnetic resonance and $^{47,49}\text{Ti}$ and ^{207}Pb nuclear magnetic resonance (NMR) measurements are carried out in PbTiO_3 single crystals at temperatures from 300 K down to 20 K. It was found that the tetragonal crystal-field parameter of the Mn^{4+} and Cr^{3+} impurity ions undergoes an unexpected change in its temperature dependence at $T < 170$ K: it increases with decreasing temperature to 150–170 K and then strongly decreases with further temperature lowering. Electric-field gradient at Ti site measured from $^{47,49}\text{Ti}$ NMR shows nonuniform change with decreasing temperature: it sharply increases with decreasing temperature to 150–170 K and is practically temperature independent below these temperatures. Moreover, substantial broadening of NMR linewidth is seen for Ti and Pb nuclei at $T < 170$ K due to essential increase of lattice parameters fluctuations. All these facts may indicate proximity of a transition to another phase with barely perceptible crystal-structure modification as reported in the paper by Kobayashi *et al.* [*Phys. Rev. B* **28**, 3866 (1983)] while, actually, it was not detected in NMR. The experimental data are compared with those obtained from *ab initio* calculations.

DOI: [10.1103/PhysRevB.107.104107](https://doi.org/10.1103/PhysRevB.107.104107)

I. INTRODUCTION

Lead titanate (PbTiO_3) is one of the well-studied ferroelectric materials [1] widely used in electronic technique. It has a simple cubic perovskite structure at $T > 763$ K which transforms into the tetragonal $P4mm$ polar structure below this temperature [2]. The ferroelectric phase transition is of the first order with the ratio of lattice constants $c/a = 1.06$ at 296 K [3]. Besides the importance of the applications of this material as ferroelectrics and piezoelectrics [4], its physical properties are still attracting much attention from scientists. In particular, PbTiO_3 - SrTiO_3 epitaxial superlattices with ferroelectric vortices and skyrmions were recently developed [5,6]. These polar textures are considering as promising hosts for electron spins which can be manipulated by electric fields [7,8] with potential implications for spin-based nanoelectronics and quantum sensing and computing [9].

One of the most interesting problems in PbTiO_3 , that has not yet been completely solved, is whether this ferroelectric material undergoes other transition (or transitions) at low temperatures like many other ferroelectric perovskites, e.g., BaTiO_3 , KNbO_3 , and NaNbO_3 [1,10]. There have been many attempts to detect another polar structure in PbTiO_3 , different from the tetragonal one. The first report concerning this problem was given by Kobayashi and Ueda [11]. Their x-ray data showed a distinct transition at 173 K in a PbTiO_3 powder sample, with an associated decrease in the unit-cell volume and the appearance of superlattice lines. The appearance of

superlattice lines suggests that PbTiO_3 may transform into an antiferroelectric structure at 173 K. Further detailed x-ray, thermal, and piezoelectric studies have indicated a possible transition into a new tetragonal phase at around 113 K [12]. However, no superlattice lines below 173 K were observed in this study. Measurements of the perturbed γ - γ directional correlation for the first excited state of ^{44}Sc in polycrystalline sample also indicate the possibility of the occurrence of other transitions [13]. On the other hand, very careful structural investigation of powdered PbTiO_3 by neutron diffraction at 90, 158, 298, and 823 K did not find evidence for the reported low-temperature phase transitions [3]. It was, however, noted that the low-temperature isotropic temperature factors of the constituent atoms have a small maximum at around 173 K, which could be conceived as the proximity of a transition to another phase near 173 K. However, later x-ray dilatometric and optical measurements on single crystals from the same authors [14] did not show any evidence of structural changes in this low-temperature region. Finally, accurate measurements of the lattice parameters and the anisotropy of the optical susceptibilities of PbTiO_3 single-domain crystals showed that PbTiO_3 undergoes a phase transition at 183 K between C_{4v} and C_{2v} point groups [15]. This transition is of second order and the direction of polarization remains unchanged. Lattice and optical anisotropies featuring the C_{2v} phase are smaller than those ever found in other perovskite-type crystals. The a/b ratio deviation from unity is only 1.3×10^{-4} at 79 K [16]. In the opinion of the authors of Ref. [15], such extremely small lattice anisotropy in the (001) plane

could be the reason why it has been overlooked in previous investigations.

The low-temperature structure of PbTiO_3 was also investigated by magnetic resonance techniques. Our early electron paramagnetic resonance (EPR) study showed that the axial symmetry crystal-field term b_2^0 for the Cr^{3+} impurity undergoes a quite unusual change with temperature below 150–170 K [17]. It increases linearly on cooling to 170–180 K and then the b_2^0 value strongly decreases on further cooling. Such unusual temperature behavior of the local crystal field was explained as a manifestation of local configurational instability of the Cr^{3+} in PbTiO_3 lattice. This process can be triggered by a small lattice structure transformation seen by x-ray diffraction in Ref. [16]. There was an attempt to identify the lowering of symmetry of PbTiO_3 from measurements of ^{207}Pb NMR spectra [18]. However, due to the use of a powdered sample and the resulting broad spectrum, it was impossible to distinguish the extremely small deviations from tetragonal symmetry from that proposed in Ref. [15].

As can be seen from this brief survey, the low-temperature ground state structure of PbTiO_3 is far from being well understood. These early data on the low-temperature PbTiO_3 structure need further independent confirmation using also other experimental techniques, especially those sensitive to small changes in the crystal structure.

In the present paper, we present the results of our detailed investigation of PbTiO_3 low-temperature structure by using EPR and NMR techniques. Both these spectroscopies belong to the most successful techniques for studying phase transitions [19]. Most of the measurements were performed on high-quality single crystals, which were previously studied in Refs. [17,20]. We found that the temperature dependence of the tetragonal crystal-field parameter, derived from the Cr^{3+} and Mn^{4+} EPR spectra, shows an anomaly around 170–175 K suggesting a change position of these ions in lattice. Furthermore, we also present NMR data for $^{47,49}\text{Ti}$ isotopes measured in PbTiO_3 single crystals in the wide temperature region, 40–290 K. Unusually strong increase of NMR linewidth below 170 K for both $^{47,49}\text{Ti}$ isotopes is accompanied by a marked change in the slope of the temperature dependence of electric-field gradient at the Ti^{4+} ion. This may indicate barely perceptible low-temperature crystal-structure modification in PbTiO_3 like described in Ref. [15]. The experimental study is accompanied by the density-functional theory (DFT) calculations.

II. EXPERIMENTAL

We have studied two types of PbTiO_3 single crystals grown by a flux method; both were nominally pure undoped crystals. The first type of crystals (SC1) was in the form of thin $5 \times 4 \times 0.2$ -mm³ plates. These crystals contained a small amount of Cr^{3+} and Fe^{3+} paramagnetic ions (~ 25 – 50 ppm). The second type of crystals (SC2) had a rectangular shape, size $3 \times 2 \times 1.5$ mm³, and contained Mn^{4+} , Fe^{3+} , and Cr^{3+} impurities (~ 20 – 50 ppm). Both types of the crystals had 180° domains, with the c axis perpendicular to the larger crystal surface. The domain structure was checked using a polarization microscope. The content of the a -type 90° domains was less than 1% and their relative concentration could be easily

calculated from EPR spectra because the spectral lines from the a - and c -type domains are well separated.

EPR measurements were performed with the Bruker EPR spectrometer EMX plus operating at 9.2–9.8 GHz. An Oxford Instrument ESR900 cryostat was used for the temperature measurements in the range from 10 to 300 K with the stability ± 0.05 K.

The room-temperature $^{47,49}\text{Ti}$ NMR spin-echo spectra of a single crystal and powdered single crystal of PbTiO_3 were recorded on a 400-MHz commercial Bruker Avance II NMR spectrometer (Larmor frequency 22.54 MHz, magnetic field ≈ 9.40 T). To obtain the spectrum of the powdered sample, 128 000 scans with a delay of 0.5 s between the scans were collected. Low-temperature measurements of $^{47,49}\text{Ti}$ (Larmor frequency 28.1815 MHz) and ^{207}Pb (Larmor frequency 104.3305 MHz) NMR spectra were performed using a 500-MHz Bruker Avance III HD NMR spectrometer at the magnetic field ≈ 11.75 T equipped with a Janis cryostat designed for NMR spectroscopy. In case of $^{47,49}\text{Ti}$, from 6000 to 20 000 scans were accumulated at every temperature with delays ranging from 1.4 to 5.8 s depending on the temperature. A four-phase “exorcycle” phase sequence (xx , xy , $x-x$, $x-y$) was used in all experiments to form echoes with minimal distortions due to antiechoes, ill-refocused signals, and piezoresonances [21]. In ^{207}Pb measurements the delay time between scans increased from 50 s at room temperature up to 600 s at 70 K.

DFT calculations were performed using the full-potential all-electron local-orbital (FPLO) code [22]. We have used the default FPLO basis. The exchange and correlation potential of Ref. [23] has been used for local- (spin-) density approximation (LDA). The potential of Ref. [24] was employed for generalized gradient approximation (GGA) functional. Electric-field gradient (EFG) and chemical-shielding parameters were calculated using WIEN2K [25], a full-potential all-electron code using augmented plane wave + local orbitals method. The size of the basis set was 1570 ($RK_{\text{MAX}} = 9.0$) with atomic sphere radii for Pb, Ti, and O chosen as 2.5, 1.7, and 1.54 atomic units, respectively. Mesh of 125 k points (division $10 \times 10 \times 9$) in the irreducible part of the Brillouin zone was used and the same variant of GGA functional as in FPLO calculations was employed. NMR chemical-shielding tensors were calculated within a linear response theory using enhanced basis and additional shifted k meshes in all six directions [26].

III. EXPERIMENTAL RESULTS

A. Cr^{3+} , Mn^{4+} , and Fe^{3+} EPR data

As an example, Fig. 1 presents EPR spectrum taken at 25 K in the SC2 sample which contains spectral lines of Cr^{3+} , Mn^{4+} , and Fe^{3+} ions. Spectra of all these ions were already described in Refs. [17,20,27–30]. In particular, only a single center is created by Cr^{3+} and Mn^{4+} ions, while Fe^{3+} creates three centers. The Fe^{3+} centers numbering in Fig. 1 is the same as in Ref. [27]. However, we prefer to assign center 2 to the isolated Fe^{3+} ions in contrast to Ref. [27], where this center was assigned to the Fe^{3+} ion in the vicinity of oxygen vacancy, $\text{Fe}^{3+}\text{-V}_\text{O}$. Our main argument is related to

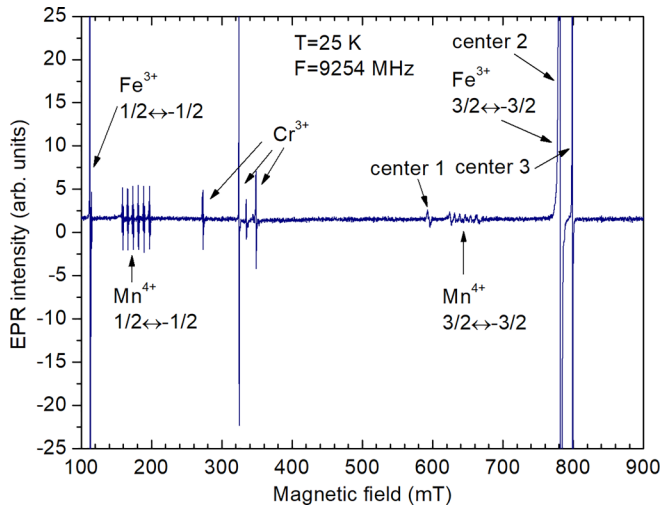


FIG. 1. EPR spectrum measured in the SC2 sample at 25 K and magnetic-field orientation normal to the c axis. The observed spectral lines are assigned to Fe^{3+} (three centers), Mn^{4+} (one center), and Cr^{3+} (one center) ions.

the fact that the tetragonal crystal-field constant of the center 2 approaches zero when the temperature increases to the cubic-tetragonal phase transition [20]. Spin-Hamiltonian parameters of these three paramagnetic ions in PbTiO_3 which substitute for Ti^{4+} are well known [17,20,27–30]. In this paper, we studied the temperature dependence of the axial crystal-field constant b_2^0 of these ions at $T < 300$ K.

The crystal-field constant b_2^0 was derived from the measured spectra using the conventional spin Hamiltonian that includes the Zeeman interaction between electron spins S and the applied magnetic field B , and crystal-field terms:

$$\mathbf{H} = \beta \mathbf{S} \cdot \mathbf{g} \cdot \mathbf{B} + \mathbf{H}_{CF}. \quad (1)$$

Here, β is the Bohr magneton and \mathbf{g} is g -tensor. The crystal-field (CF) terms can be expressed using electron spin polynomials (Stevens spin operators O_l^m) [31]. For the C_{4v} tetragonal phase of PbTiO_3 these terms have the form

$$\mathbf{H}_{ZFS} = \frac{1}{3}b_2^0\mathbf{O}_2^0 + \frac{1}{60}(b_4^0\mathbf{O}_4^0 + b_4^4\mathbf{O}_4^4), \quad (2)$$

where b_l^m are crystal-field parameters. For Cr^{3+} and Mn^{4+} ions ($3d^3$, $S = 3/2$), the second CF term is zero. For Fe^{3+} ($3d^5$, $S = 5/2$), this term is nonzero, but both b_4^0 and b_4^4 (~ 0.004 – 0.03 cm^{-1}) are much smaller than the axial constant b_2^0 ($\sim 1 \text{ cm}^{-1}$). Note that the electron-nuclear hyperfine interaction of ^{55}Mn and ^{53}Cr isotopes (for instance, six ^{55}Mn hyperfine lines are well seen at spin transitions of Mn^{4+} in Fig. 1) was not included in the spin Hamiltonian (1) as we were interested in determination of only temperature dependence of the b_2^0 crystal-field constant.

The crystal-field splitting of energy levels is larger than the microwave frequency. Thus, only two transitions can be measured for Fe^{3+} and Mn^{4+} ions as shown in Fig. 1, the central one $-1/2 \leftrightarrow 1/2$ and the forbidden $-3/2 \leftrightarrow 3/2$ (this forbidden transition is well seen at magnetic-field orientation normal to the c axis, but vanishes in intensity when magnetic field deviates from this direction). Resonance fields of these transitions were fitted by the calculated ones using the

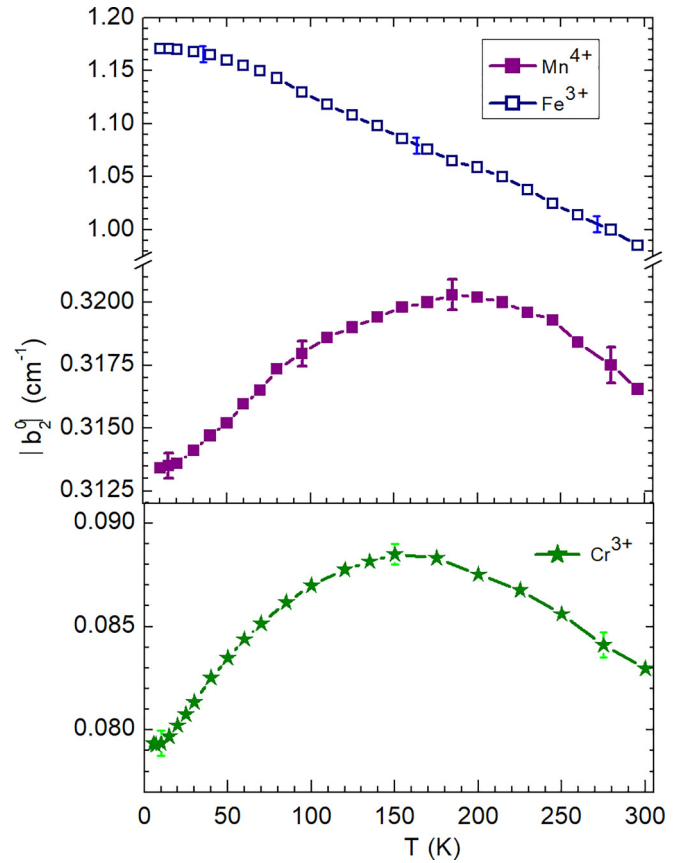


FIG. 2. Temperature dependences of the axial crystal-field constant b_2^0 for Cr^{3+} , Mn^{4+} , and Fe^{3+} measured in the SC2 crystal.

exact numerical solution of the spin Hamiltonian (1). The fit allowed an accurate determination of the b_2^0 constant and its temperature dependence. As starting parameters in the fitting procedure, we have used the spin-Hamiltonian parameters that were accurately determined at room temperature in Refs. [20] and [27]. Note that in the fitting procedure for Fe^{3+} , the cubic b_4^0 , and b_4^4 crystal-field constants were fixed, as they are almost temperature independent [27]. Since all three transitions allowed for the spin-3/2 are observed in the spectra of Cr^{3+} , its axial constant b_2^0 was directly calculated from the distance between two $\pm 1/2 \leftrightarrow \pm 3/2$ transitions at $B \parallel [001]$.

Figure 2 shows the temperature dependences of the axial crystal-field constant b_2^0 for Mn^{4+} , Cr^{3+} , and Fe^{3+} ions measured in the same crystal.

One can see that the crystal-field strength increases for all three ions when the temperature decreases down to 160–200 K in agreement with the temperature changes of lattice parameters [3]. However, below this temperature, the behavior of the constant b_2^0 for Cr^{3+} and Mn^{4+} ion strongly deviates from that of the Fe^{3+} ion: it strongly decreases on further cooling in contrast to the one expected in the tetragonal phase of PbTiO_3 (b_2^0 has to be proportional to $c/a - 1$, like for Fe^{3+}). This indicates that at low temperatures the crystal field changes not only due to the change of the c/a ratio but also due to individual shifts of ions. It could be due to a change of the local crystal field specifically for these ions, as was proposed for Cr^{3+} in Ref. [17], or it can reflect the global change in the crystal

structure with temperature. It is well known, for instance from BaTiO₃ studies [32–34], that the Mn⁴⁺ and Cr³⁺ ions, which substitute for the Ti⁴⁺, follow the shift of the Ti⁴⁺ at phase transitions in Ti-containing perovskites (this is also confirmed by our DFT calculations for Mn⁴⁺ presented in Sec. III C: DFT modeling), whereas the Fe³⁺ remains centered in the oxygen octahedron. Moreover, the Fe³⁺ ion in PbTiO₃ can additionally be stabilized by a charge-compensating defect [27]. Therefore, EPR parameters of this ion reflect mainly the change of the lattice constants with temperature, namely the tetragonality c/a . However, even for the Fe³⁺ a small deviation in the slope of the $b_2^0(T)$ is seen at 180–190 K (Fig. 2) probably due to a small shift of Fe in oxygen octahedron. Thus, we can conclude that, at least, Mn⁴⁺ and Cr³⁺ ions undergo anomalous shifts in oxygen octahedron. Taking into account that the crystal-field parameters of two different impurity ions, Mn⁴⁺ and Cr³⁺, at Ti⁴⁺ position show completely the same temperature behavior, we can suppose similar behavior in the displacement of Ti⁴⁺ host ions at $T < 170$ K. Surprisingly, exactly at the temperature region where the anomalies in Mn⁴⁺ and Cr³⁺ spectra are seen, x-ray diffraction detected the appearance of the small difference between a - and b lattice constants [15,16]. However, because the measured ratio $a/b - 1 \approx 1.3 \times 10^{-4}$ is so small, it could not be detected in EPR spectra. The expected Mn⁴⁺ resonance line shift (about 0.5–0.6 mT) due to possible rhombicity is within linewidth which is 2–3 mT for the $3/2 \leftrightarrow -3/2$ transition which is quite sensitive to small ionic shifts. Also, usual mismatch in crystal orientation of only 1° – 2° leads to the resonance field shift of 2–3 mT. To clarify the situation with Ti displacement we measured NMR spectra of two titanium isotopes, ⁴⁷Ti and ⁴⁹Ti.

B. ^{47,49}Ti and ²⁰⁷Pb NMR data

Titanium nucleus has two NMR active isotopes with different spins and quadrupole moments: ⁴⁷Ti ($I = 5/2$, $Q = 30.2$ fm², natural abundance 7.44%) and ⁴⁹Ti ($I = 7/2$, $Q = 24.7$ fm², natural abundance 5.41%). Both these isotopes undergo interaction of their quadrupole moments with the electric-field gradients. The spin Hamiltonian of these nuclei contains thus additional term \mathbf{H}_Q , which describes the quadrupole interaction:

$$\mathbf{H} = \mathbf{H}_Z + \mathbf{H}_{CS} + \mathbf{H}_Q, \quad (3)$$

where

$$\mathbf{H}_Q = \frac{C_Q h}{4I(2I-1)} \left[3\mathbf{I}_z^2 - I^2 + \frac{\eta}{2}(\mathbf{I}_+ + \mathbf{I}_-) \right], \quad (4)$$

and $C_Q = e^2 q Q / h$ is the quadrupole coupling constant which is proportional to the largest eigenvalue $V_{zz} = eq$ of the EFG tensor, whereas η is the asymmetry parameter which measures the EFG biaxiality: $\eta = (V_{xx} - V_{yy}) / V_{zz}$. \mathbf{H}_Z and \mathbf{H}_{CS} are the Zeeman and chemical-shielding (chemical-shift) (CS) terms of the spin Hamiltonian. For the ²⁰⁷Pb nucleus (nuclear spin $I = 1/2$, natural abundance 22.6%), NMR frequency is determined by the Hamiltonian which contains only the Zeeman \mathbf{H}_Z and chemical-shielding \mathbf{H}_{CS} terms.

As an example, Fig. 3 presents ^{47,49}Ti NMR spectrum measured in the SC2 sample at temperatures from 270 K

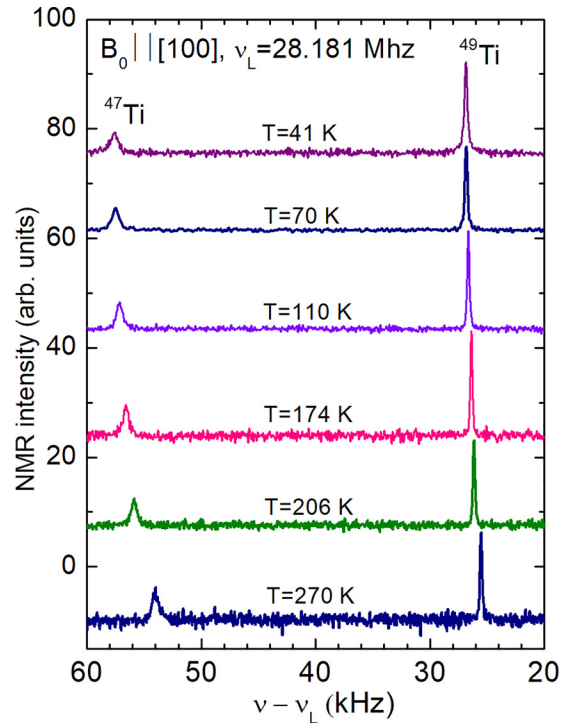


FIG. 3. Temperature dependence of ^{47,49}Ti NMR spectrum in PbTiO₃ crystal with $\mathbf{B} \parallel [100]$.

down to 41 K, with [100] axis parallel to the static magnetic field \mathbf{B} . The Ti spectra were referenced against the secondary standard of SrTiO₃, which is cubic and produces a narrow ⁴⁹Ti resonance, taken here as the zero for the chemical shift. Only two spectral lines corresponding to the $1/2 \leftrightarrow -1/2$ central transition of the ⁴⁷Ti and ⁴⁹Ti nuclei are seen in the NMR spectrum of PbTiO₃. The other (satellite) transitions were not acquired due to their much larger linewidth and correspondingly much smaller intensity.

Because the $1/2 \leftrightarrow -1/2$ NMR transition is not shifted by the quadrupole interaction in the first order, the second-order quadrupole shift of this transition with respect to the Larmor frequency ν_L has to be considered and is given by [35,36]

$$\begin{aligned} \nu_{1/2}^{(2)} = & -\frac{C_Q^2}{16\nu_L} \left(I(I+1) - \frac{3}{4} \right) f_\eta(\theta, \varphi) \\ & + \nu_L \left[\begin{array}{l} \delta_{iso} + \delta_{ax}(3\cos^2\theta - 1) \\ + \delta_{aniso}\sin^2\theta \cos 2\varphi \end{array} \right], \end{aligned} \quad (5)$$

where the chemical-shift contribution is also included [last term in Eq. (5)]. δ_{iso} , δ_{ax} , and δ_{aniso} are isotropic, axial, and anisotropic components of the chemical shift. They are defined as $\delta_{iso} = 1/3(\delta_{xx} + \delta_{yy} + \delta_{zz})$; $\delta_{ax} = 1/6(2\delta_{zz} - \delta_{yy} - \delta_{xx})$; and $\delta_{aniso} = 1/2(\delta_{yy} - \delta_{xx})$ [36]. Angles θ and φ are the Euler angles of the external magnetic field referenced to the principal x , y , and z -axes system of the EFG and CS tensors. The function $f_\eta(\theta, \varphi)$ has a cumbersome form and its actual expression was presented in a previous study [36]. For the tetragonal symmetry of PbTiO₃ (at $\eta = 0$), the function $f_\eta(\theta, \varphi)$ has a simple form:

$$f_\eta(\theta) = (1 - \cos^2\theta)(9\cos^2\theta - 1). \quad (6)$$

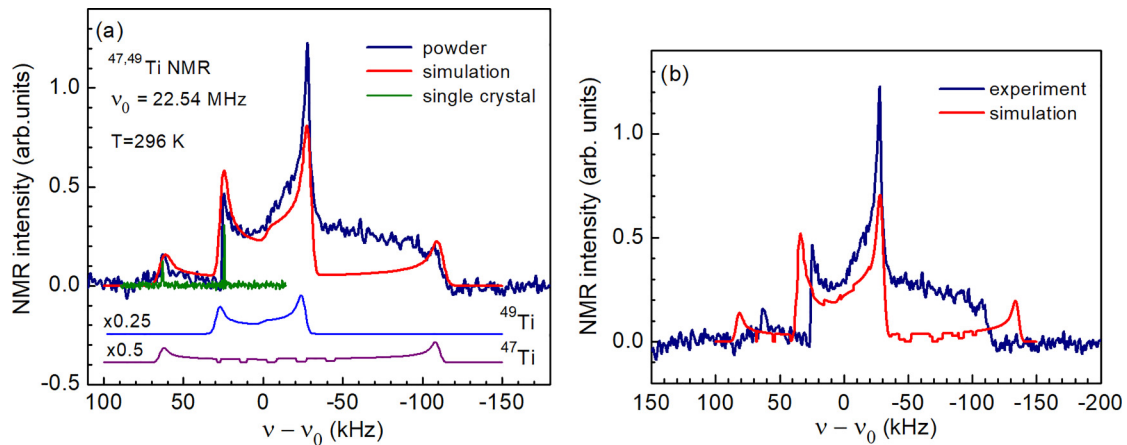


FIG. 4. (a) $^{47,49}\text{Ti}$ NMR spectrum in the powdered sample (blue line) of PbTiO_3 and its simulated spectrum (red line). For comparison, the single-crystal $^{47,49}\text{Ti}$ spectrum at $B \parallel [100]$ is shown as well (green line). Thin solid lines show separate contributions from the ^{47}Ti and ^{49}Ti isotopes. (b) Measured and calculated spectrum using parameters from Ref. [38]. All spectra are taken at 296 K.

By using the fact that the CS parameters must be the same for the two Ti isotopes (see, e.g., Ref. [37]), it was possible to calculate the quadrupole constant C_Q from the two lines of the central transition spectrum. As a starting point, we first fitted the spectrum from the powdered sample. Figure 4 shows such powder spectrum together with its simulation and a single-crystal spectrum taken at 296 K. Both powder and single-crystal spectra were simulated [Fig. 4(a)] using the following parameters: $C_Q(^{47}\text{Ti}) = 11.00$ MHz, $C_Q(^{49}\text{Ti}) = 8.997$ MHz, $\delta_{ax} = -150$ ppm, and $\delta_{iso} = 170$ ppm. These parameters give a good agreement between the experimental and the calculated peak positions for both ^{47}Ti and ^{49}Ti isotopes. We note that the measured spectrum contains a broad feature related to artifacts in the spin-echo signal. The quadrupolar parameters determined here differ noticeably from those reported in Ref. [38], where $C_Q(^{49}\text{Ti}) = 9.98$ MHz was found and the CS anisotropy was not taken into account. For comparison, in Fig. 4(b) we present the calculated spectrum with $C_Q(^{49}\text{Ti}) = 9.98$ MHz and $C_Q(^{47}\text{Ti}) = 12.20$ MHz. One can assess the difference between our measured and such a simulated spectra, especially in the positions of the ^{47}Ti peaks. Later, the data from Ref. [38] were improved by taking into account the CS anisotropy [39]. But, their $C_Q(^{49}\text{Ti}) = 9.45$ MHz still markedly differs from the value measured in this work.

The temperature dependence of the ^{47}Ti quadrupole constant determined from single-crystal spectrum assuming the tetragonal symmetry is displayed in Fig. 5. Similar behavior of the quadrupole constant was obtained for the ^{49}Ti isotope. The measurements were done down to 40 K, as below this temperature the spin-lattice relaxation time became too long for the spectrum to be collected in a feasible time.

Apparently, the electric-field gradient at Ti site undergoes a distinct change of its temperature dependence at approximately 170 K. Below this temperature, it follows well (red dot line in Fig. 5) the empirical relation (Gaussian function) [40] $C_Q(T) = C_Q(0) \exp(-\alpha T^2)$, where $C_Q(0) = 11.452$ MHz and $\alpha = 2.6 \times 10^{-7} (\text{K}^{-2})$. This formula empirically accounts for the effect of the thermal vibrations of lattice. However, at $T > 170$ K, the theoretical line strongly deviates from the experimental points as the effect of the

temperature dependent tetragonality, $c/a - 1$, becomes dominant (see, e.g., precise measurements of lattice constants in Ref. [16]).

Note that the Ti axial chemical shift is temperature insensitive, $\delta_{ax} = -150(1)$ ppm, when the temperature decreases from 300 to 40 K, while the isotropic chemical shift slightly increases (Fig. 5), reflecting change of the average Ti–O bond length at $T < 170$ K.

No visible splitting of the $^{47,49}\text{Ti}$ NMR lines is seen due to possible nonequivalence of the a and b crystal axes in the expected orthorhombic phase at $T < 170$ K. We expected here namely the splitting of NMR lines due to multidomain nature of crystals, where the a and b crystal axes are swapped. This suggests that the symmetry remains tetragonal down to 40 K within sensitivity of NMR.

To estimate the expected change in the $^{47,49}\text{Ti}$ NMR frequencies due to possible nonequivalence of the a and b crystal axes, the EFG tensor was calculated within the DFT using the WIEN2K code [26], which usually computes EFG parameters in a good agreement with the experimental values. The chemical-shielding tensor was not calculated due to its minor

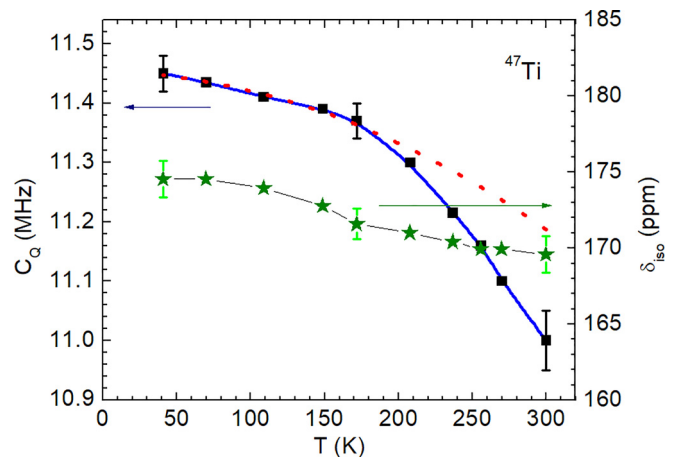


FIG. 5. Temperature dependence of the ^{47}Ti quadrupole coupling constant and the isotropic chemical shift in PbTiO_3 single crystal.

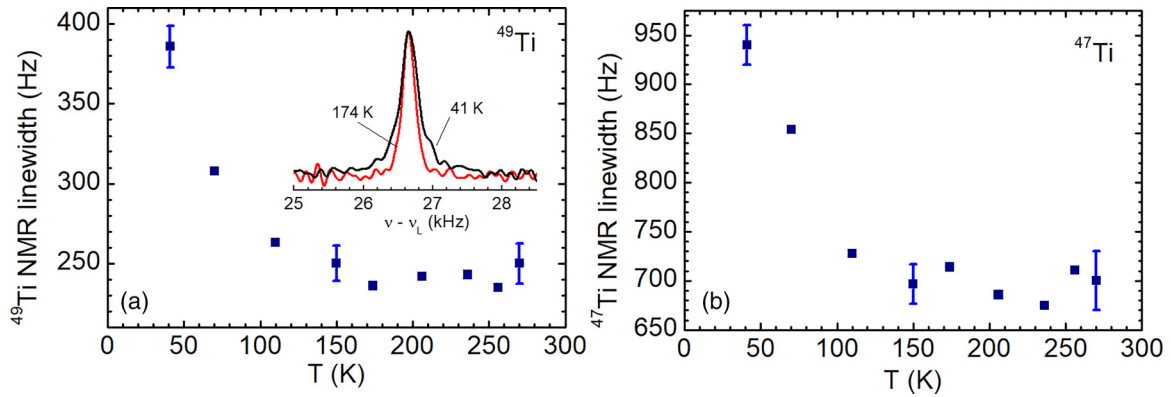


FIG. 6. Temperature dependence of the full width at half maximum (FWHM) of the ^{49}Ti (a) and ^{47}Ti (b) NMR lines measured in PbTiO_3 single crystal for $\mathbf{B} \parallel [100]$. Inset in the graph (a) shows the ^{49}Ti NMR spectral line at 174 and 41 K normalized to the same peak intensity.

effect on NMR spectrum. The results of the calculations are presented in Fig. 9 of the Appendix. In particular, the EFG asymmetry parameter η linearly increases with increase of the $a/b-1$ ratio. For the reported $a/b-1 = 1.3 \times 10^{-4}$ [15], the calculated parameter η is only 0.01. This corresponds to NMR frequency shift of only 0.5 and 0.16 kHz for ^{47}Ti and ^{49}Ti nuclei, respectively. Such small frequency shifts can in principle be certainly distinguished in experiment as the linewidth is 0.7 and 0.25 kHz for both Ti isotopes, respectively. However, we observed only a marked (by 60%) increase of the NMR linewidth below 170 K (Fig. 6), indicating that fluctuations of the EFG tensor (and also chemical-shielding tensor) at Ti site substantially increase at $T < 170$ K due to anomalous fluctuation of crystal-structure parameters or Ti position in oxygen octahedron (although, usually, thermal fluctuations of EFG should only decrease when the temperature decreases). Thus, our result agrees with that reported in Ref. [3], where unexpected increase of the Ti and O isotropic temperature factors was observed at 160–110 K in the neutron-diffraction spectra.

For the ^{207}Pb nucleus (nuclear spin $I = 1/2$, natural abundance 22.6%), the NMR frequency is determined by the Hamiltonian which contains only the Zeeman \mathbf{H}_Z and chemical-shift \mathbf{H}_{CS} terms. Therefore, NMR line shift with temperature with respect to the Larmor frequency depends only on the chemical-shift parameters. As an example, Fig. 7 presents separated ^{207}Pb NMR spectra measured simultaneously in two crystals for different temperatures.

The two single crystals were in mutually perpendicular orientations: one crystal with c axis approximately perpendicular to the external magnetic field ($\mathbf{B} \parallel [100]$, line on the right side in Fig. 7) and the other crystal with c axis approximately parallel to the field ($\mathbf{B} \parallel [001]$, left-side line). The spectra were referenced against the resonance frequency of $\text{Pb}(\text{NO}_3)_2$ standard. The reason for such arrangement of the crystals was to record lines from two crystal orientations at the same time (during one measurement) for each temperature. It allows a more accurate comparison of resonance frequencies at a monitored temperature and avoids the inaccuracies that would arise in successive measurements of the sample in different orientations. Then, the chemical-shift parameters can be easily calculated by using a simple relation which connects these

parameters with resonance frequency:

$$\nu - \nu_L = \nu_L [\delta_{iso} + \delta_{ax}(3\cos^2\theta - 1) + \delta_{aniso}\sin^2\theta \cos 2\varphi], \quad (7)$$

where δ_{iso} and δ_{ax} are the dominant values. It is expected that δ_{aniso} could be nonzero at $T < 150$ – 170 K due to inequality of the δ_{xx} and δ_{yy} values ($a/b \neq 1$). However, as in case of Ti NMR, there is no visible splitting of the ^{207}Pb NMR line at $T < 150$ – 170 K that could indicate an orthorhombic distortion. We expected namely the splitting of NMR lines due to multidomain nature of crystals.

Temperature dependence of the axial chemical-shift parameter of ^{207}Pb nuclei and the ^{207}Pb linewidth show similar

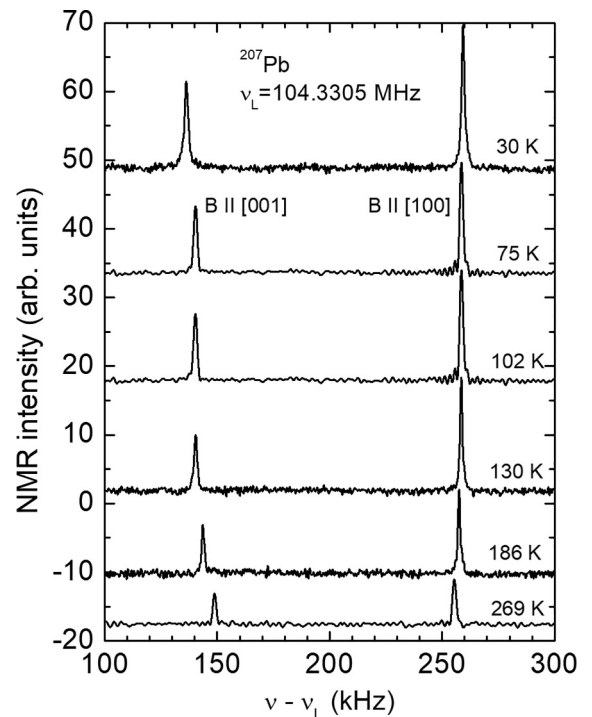


FIG. 7. Temperature dependence of ^{207}Pb NMR spectrum in PbTiO_3 crystal with $\mathbf{B} \parallel [001]$ (left-side line) and $\mathbf{B} \parallel [100]$ (right-side line). Accuracy of the crystal orientations is about 10° .

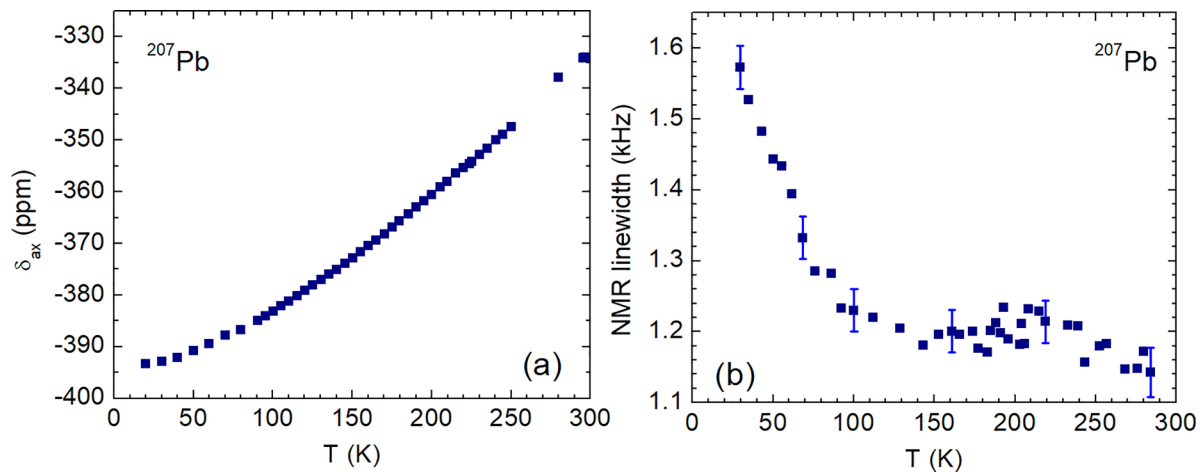


FIG. 8. (a) Temperature dependence of the ^{207}Pb axial chemical shift component and (b) NMR linewidth at $B \parallel [100]$.

behavior with temperature as in the case of Ti spectrum. This is illustrated in Fig. 8.

Similarly to Ti NMR, marked increase of ^{207}Pb NMR linewidth is seen below approximately 150 K. DFT calculations [see the Appendix, Fig. 9(b)] predicts that in case of the small rhombicity $a/b-1 = 1.3 \times 10^{-4}$ the difference $\delta_{xx} - \delta_{yy}$ is only 1.3–1.4 ppm that can lead to an NMR line shift at 50–100 Hz only. Such small shift in resonance frequency cannot be resolved in spectrum as the linewidth is much bigger. The broadening of NMR line at $T < 150$ K can be explained by temperature-dependent fluctuations of the chemical-shielding tensor which reflects fluctuations of crystal parameters (in particular chemical bonds). These fluctuations abnormally increase at $T < 150$ K.

C. DFT modeling

Density-functional theory allows calculating the ground state structure parameters by minimizing the total energy functional. The functional is not known exactly, and the result depends on its approximate form. In Ref. [41], the calculations using local-density approximation have shown no instability of the tetragonal structure with respect to orthorhombic distortions. The generalized gradient approximation functional,

introduced later [24], gives structural parameter values that are closer to experiment [42] compared to LDA. That is why we have performed a set of calculations using an all-electron code for both the LDA and GGA functionals. For both functionals, like in the previous calculations [41], we have confirmed the tetragonal ground state structure.

In Ref. [3], the structure of PbTiO_3 at several temperatures was determined by the Rietveld neutron powder profile method. The authors have not detected the tiny splitting in the a lattice parameter at low temperatures, but they have reported the coordinates of all atoms within the unit cell (see Table II of Ref. [3]). The coordinates may be written as Pb at $(0, 0, \delta z_{\text{Pb}})$, Ti at $(1/2, 1/2, 1/2 + \delta z_{\text{Ti}})$, O(1) at $(1/2, 1/2, \delta z_{\text{O}(1)})$, O(2) at $(1/2, 0, 1/2)$, and O(3) at $(0, 1/2, 1/2, \delta z_{\text{O}(3)})$. In the tetragonal phase, coordinates for O(2) and O(3) are identical as $\delta z_{\text{O}(3)} = 0$. In our notations, the O(2) sublattice remains unshifted in the ferroelectric phase. This is different from the notations of Ref. [3], where the Pb ion is at the origin. We have used the lattice parameters reported in Ref. [3] for every temperature as an input and have calculated the coordinates of the atoms within the unit cell corresponding to the energy minimum. The results shown in Tables I and II for LDA and GGA functionals reproduce the dependence of Ti shift on

TABLE I. Values of ion shifts from ideal positions for the tetragonal unit-cell parameters corresponding to various temperatures. Comparison of DFT results and experiment [O(2) at origin]. Second column gives the results calculated for the orthorhombic ground-state structure.

	0 K (LDA)	90 K		158 K		298 K	
	$a = 3.8756 \text{ \AA}$	$a = 3.895 \text{ \AA}$		$a = 3.899 \text{ \AA}$		$a = 3.905 \text{ \AA}$	
	$b = 3.8744 \text{ \AA}$	$c = 4.171 \text{ \AA}$		$c = 4.167 \text{ \AA}$		$c = 4.156 \text{ \AA}$	
	$c = 4.081 \text{ \AA}$	$c/a = 1.071$		$c/a = 1.068$		$c/a = 1.064$	
	$c/a = 1.053$						
	$V = 61.2787 \text{ \AA}^3$						
	LDA	Exp.	LDA	Exp.	LDA	Exp.	
δz_{Ti} (\AA)	0.2877	0.3310	0.338	0.3291	0.331	0.3241	0.324
δz_{Pb} (\AA)	0.3991	0.4830	0.505	0.4827	0.504	0.4784	0.486
$\delta z_{\text{O}(1)}$ (\AA)	0.0336	0.0145	0.013	0.0146	0.025	0.0155	0.013
$\delta z_{\text{O}(3)}$ (\AA)	0.0005	0	0	0	0	0	0

TABLE II. Ion shifts calculated analogous to Table I, but with the use of GGA functional.

Ion shift	0 K (GGA)	90 K	158 K	298 K
		$a = 3.9657 \text{ \AA}$ $b = 3.9187 \text{ \AA}$ $c = 4.2990 \text{ \AA}$ $c/a = 1.084$ $a/b = 1.012$ $V = 66.8099$	$a = 3.895 \text{ \AA}$ $c = 4.171 \text{ \AA}$ $c/a = 1.071$	$a = 3.899 \text{ \AA}$ $c = 4.167 \text{ \AA}$ $c/a = 1.068$
$\delta z_{\text{Ti}} (\text{ \AA})$	0.3757	0.3121	0.3102	0.3046
$\delta z_{\text{Pb}} (\text{ \AA})$	0.5442	0.4097	0.4092	0.4040
$\delta z_{\text{O}(1)} (\text{ \AA})$	-0.0077	0.0176	0.0179	0.0183
$\delta z_{\text{O}(3)} (\text{ \AA})$	0.0149	0	0	0

temperature. The second column in every table presents the atom coordinates for the orthorhombic ground state which are, however, far from experimental values.

In order to simulate the isovalent substitution of Mn^{4+} for Ti^{4+} , we have performed calculation for $2 \times 2 \times 2$ $\text{Pb}_8\text{MnTi}_7\text{O}_{24}$ 40-atom supercell. Starting with atomic positions determined for a single cell in the previous calculations, we have relaxed the Mn position as well as the positions of six surrounding oxygen atoms. The results are shown in Table III and confirm the off-central position of Mn. The oxygen octahedral cage around Mn is contracted, compared to the octahedra surrounding Ti ions.

In contrast to the Mn^{4+} substitution for Ti^{4+} host ion, Fe^{3+} and Cr^{3+} are charged defects. Their excess charge must be compensated by another defect in order to keep the electroneutrality. For example, an oxygen vacancy can compensate two Fe^{3+} ions. Such $\text{Fe}^{3+}\text{-V}_\text{O}\text{-Fe}^{3+}$ complexes were simulated using DFT calculations of the $2 \times 2 \times 2$ supercell in Ref. [43]. However, when the compensating defects are situated far away from the EPR center to make small disturbance to impurity ion, the adequate modeling of such situation demands an enormous supercell, which is not reachable for the present-day DFT codes.

IV. CONCLUSIONS

Detailed measurements of Fe^{3+} , Cr^{3+} , and Mn^{4+} EPR spectra were carried out in single crystals of the classical ferroelectric PbTiO_3 at temperatures from 300 K down to

20 K. It was found that the crystal-field splitting parameter b_0^2 of all these impurity ions changes nonmonotonically with decreasing temperature. Moreover, for two of these ions, Cr^{3+} and Mn^{4+} , the axial crystal-field parameter has a distinct maximum at 150–170 K and strongly decreases below these temperatures, suggesting temperature instability of these paramagnetic ions at the octahedral sites.

$^{47,49}\text{Ti}$ and ^{207}Pb NMR spectra were measured in the same crystals at temperatures 40–300 K. It was found that the quadrupole constant of the two Ti isotopes undergoes a distinct change of slope in its temperature dependence: while it sharply increases with decreasing temperature to 150–170 K, below these temperatures it is practically temperature independent. Moreover, the Ti NMR data show that EFG tensor at Ti site undergoes large fluctuations below approximately 150–170 K reflecting in the marked increase of NMR linewidth. The same broadening is seen for ^{207}Pb NMR line as well, suggesting that lattice parameters are also undergoing essential fluctuations below 150–170 K, like in SrTiO_3 at approaching the antiferrodistortive transition at 105 K [44]. This may indicate the proximity of a transition to another phase in PbTiO_3 which, however, was not detected in NMR. DFT calculation of the NMR parameters (EFG and chemical-shielding tensors) predicts that the expected NMR line splitting or shift due to possible weak rhombicity ($a/b-1 = 1.3 \times 10^{-4}$, Ref. [15]) is within linewidth and cannot be definitely detected in experiment even for single crystal.

The isovalent substitution of Mn^{4+} for Ti^{4+} has been simulated as well using the initial atomic positions of lattice

TABLE III. Values of Mn impurity ion and surrounding oxygen shifts from ideal positions for the tetragonal unit-cell parameters corresponding to various temperatures.

Ion shift	90 K	158 K	298 K
		$a = 3.895 \text{ \AA}$ $c = 4.171 \text{ \AA}$ $c/a = 1.071$	$a = 3.899 \text{ \AA}$ $c = 4.167 \text{ \AA}$ $c/a = 1.068$
$\delta z_{\text{Mn}} (\text{ \AA})$	0.2220	0.2229	0.2190
$\delta z_{\text{O}(1)} (\text{ \AA})$ under Mn	0.0242	0.0243	0.0254
$\delta z_{\text{O}(1)} (\text{ \AA})$ above Mn	-0.1121	-0.0092	-0.1078
$\delta z_{\text{O}(2)} (\text{ \AA})$	-0.0007	-0.0027	-0.0019
$\delta x, y_{\text{O}(2)} (\text{ \AA})$	0.0314	0.0312	0.0310
$\delta z_{\text{Ti}} (\text{ \AA})$	0.3310	0.3291	0.3241
$\delta z_{\text{Pb}} (\text{ \AA})$	0.4830	0.4827	0.4784

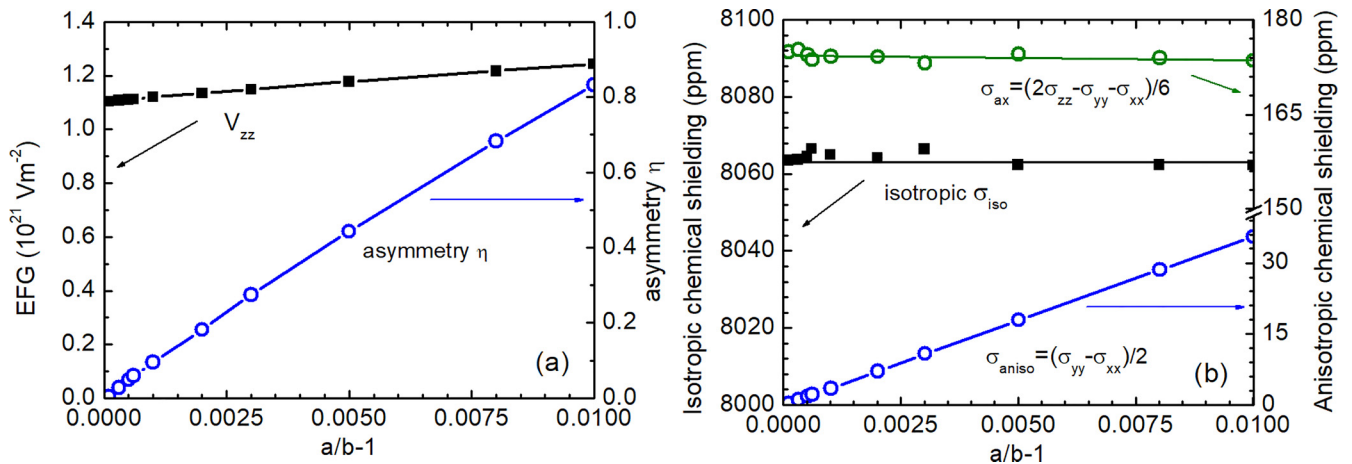


FIG. 9. Calculated dependence on the $a/b-1$ ratio for the V_{zz} and asymmetry parameter η of the EFG tensor at Ti site (a) and the chemical-shielding parameters of ^{207}Pb (b).

ions determined by neutron diffraction at temperatures 298, 158, and 90 K [3]. It was found that Mn^{4+} undergoes similar off-center shifts as the host lattice Ti^{4+} ion. This confirms that Mn^{4+} ion can be used as a good paramagnetic probe of PbTiO_3 crystal-structure transformation at phase transitions.

ACKNOWLEDGMENTS

The support of the Czech Science Foundation under Project No. 23-05578S (V.L.) is gratefully acknowledged. Computational resources were supplied by the project “e-Infrastruktura CZ” (e-INFRA LM2018140) provided within the program Projects of Large Research, Development and Innovations Infrastructures. Support by the National Academy of Sciences of Ukraine (Projects No. III-2-22 and No. III-4-23) is gratefully acknowledged. We thank Ulrike Nitzsche for technical assistance, and the IFW Dresden (Germany) for the use of their computer facilities.

APPENDIX

The PbTiO_3 ground state structure was also calculated within the DFT using the full-potential all-electrons augmented plane wave+local orbitals method implemented in

the WIEN2K code [25]. In particular, we wanted to estimate the EFG parameters for Ti (V_{zz} and asymmetry parameter η) and ^{207}Pb chemical-shielding tensor σ as a function of possible rhombicity, i.e., $a/b-1$ ratio. The results are shown in Fig. 9. One can see that the EFG asymmetry parameter for Ti and the difference in chemical shielding $\sigma_{xx} - \sigma_{yy}$ of ^{207}Pb linearly increase with increase of the orthorhombic distortion a/b . V_{zz} is about $1.1 \times 10^{21} \text{ V m}^{-2}$ and slightly increases with increase of $a/b-1$. Experimentally measured V_{zz} is larger, $1.56 \times 10^{21} \text{ V m}^{-2}$. At the same time, calculated isotropic chemical shielding of ^{207}Pb is practically constant, 8063(3) ppm, regardless of the orthorhombic deformation. Such a constant character of the σ_{iso} explains why in Ref. [18] (as well as our ^{207}Pb NMR) no changes in the ^{207}Pb isotropic shifts which could be related to the orthorhombic transition were observed. The calculated axial part of the chemical shielding in the tetragonal phase $\sigma_{ax} = 1/6(2\sigma_{zz} - \sigma_{yy} - \sigma_{xx}) = 174$ ppm is about two times smaller than the measured value 395 ppm at $T = 20$ K. It is practically independent on rhombic distortion [green circles in Fig. 9(b)]. On the other hand, as expected, the anisotropic part of the shielding tensor linearly increases with increase of the rhombic distortion [blue circles in Fig. 9(b)].

- [1] M. E. Lines and A. M. Glass, *Principles and Application of Ferroelectrics and Related Materials* (Clarendon Press, Oxford, 1977).
- [2] G. Shirane, R. Pepinsky, and B. C. Frazer, X-ray and neutron diffraction study of ferroelectric PbTiO_3 , *Acta Cryst.* **9**, 131 (1956).
- [3] A. M. Glazer and S. A. Mabud, Powder profile refinement of lead zirconate titanate at several temperatures. II. Pure PbTiO_3 , *Acta Cryst. B* **34**, 1065 (1978).
- [4] B. Jaffe, W. R. Cook, and H. Jaffe, *Piezoelectric Ceramics* (Academic Press, New York, 1971); *Physics of Ferroelectrics*, edited by K. M. Rabe, Ch. H. Ahn, and J.-M. Triscone (Springer-Verlag, Berlin, 2007).
- [5] A. K. Yadav, C. T. Nelson, S. L. Hsu, Z. Hong, J. D. Clarkson, C. M. Schlepütz, A. R. Damodaran, P. Shafer, E. Arenholz,

- L. R. Dedon *et al.*, Observation of polar vortex in oxide superlattices, *Nature (London)* **530**, 198 (2016).
- [6] S. Das, Y. L. Tang, Z. Hong, M. A. P. Goncalves, M. R. McCarter, C. Klewe, K. X. Nguyen, F. Gomez-Ortiz, P. Shafer, E. Arenholz *et al.*, Observation of room temperature polar skyrmions, *Nature (London)* **568**, 368 (2019).
- [7] J. Liu, V. Laguta, K. Inzani, W. Huang, S. Das, R. Chatterjee, E. Sheridan, S. M. Griffin, A. Ardavan, and R. Ramesh, Coherent electric field manipulation of Fe^{3+} spins in PbTiO_3 , *Sci. Adv.* **7**, eabf8103 (2021).
- [8] S. Das, V. Laguta, K. Inzani, W. Huang, J. Liu, R. Chatterjee, M. R. McCarter, S. Susarla, A. Ardavan, J. Junquera, S. M. Griffin, and R. Ramesh, Inherent spin-polarization coupling in magnetoelectric vortex, *Nano Lett.* **22**, 3976 (2022).

- [9] S. E. Crawford, R. A. Shugayev, H. P. Paudel, P. Lu, M. Syamlal, P. R. Ohodnicki, B. Chorpening, R. Gentry, and Y. Duan, Quantum sensing for energy applications: Review and perspective, *Adv. Quantum Technol.* **4**, 2100049 (2021).
- [10] G. A. Smolenskii, V. A. Bokov, V. A. Isupov, N. N. Krainik, R. E. Pasynkov, and A. I. Sokolov, *Ferroelectrics and Related Materials* (Gordon and Breach, New York, 1984).
- [11] J. Kobajashi and R. Ueda, X-ray study of phase transition of ferroelectric PbTiO₃ at low temperature, *Phys. Rev.* **99**, 1900 (1955); J. Kobajashi, S. Okamoto, and R. Ueda, Dielectric behavior of lead titanate at low temperature, *ibid.* **103**, 830 (1956).
- [12] S. Igegami, I. Ueda, and T. Miyazawa, Phase transitions of PbTiO₃ at low temperatures, *J. Phys. Soc. Jpn.* **26**, 1324 (1969).
- [13] P. Doshi, J. Glass, and M. Novotny, Low-temperature structure of PbTiO₃, *Phys. Rev. B* **7**, 4260 (1973).
- [14] S. A. Mabud and A. M. Glazer, Lattice parameters and birefringence in PbTiO₃ single crystals, *J. Appl. Cryst.* **12**, 49 (1979).
- [15] J. Kobajashi, Y. Ueda, and Y. Sakemi, X-ray and optical studied on phase transition of PbTiO₃ at low temperatures, *Phys. Rev. B* **28**, 3866 (1983).
- [16] J. Kobayashi, Y. Uesu, Y. Sakemi, and T. Hosokawa, Phase transitions of PbTiO₃ in the low temperature region, *Ferroelectrics* **37**, 571 (1981).
- [17] V. V. Laguta, T. V. Antimirova, M. D. Glinchuk, I. P. Bykov, J. Rosa, M. Zaritskii, and L. Jastrabik, Local configurational instability of Cr³⁺ in PbTiO₃, *J. Phys.: Condens. Matter* **9**, 10041 (1997).
- [18] D. A. Bussian and G. S. Habison, Variable temperature ²⁰⁷Pb NMR of PbTiO₃, *Solid State Commun.* **115**, 95 (2000).
- [19] *Magnetic Resonance of Phase Transitions*, edited by F. J. Owens, Ch. P. Poole, and H. A. Farach (Academic Press, New York, 1979).
- [20] V. V. Laguta, M. D. Glinchuk, I. P. Bykov, J. Rosa, L. Jastrabik, and Yu. L. Maksimenko, Impurity centers in PbTiO₃ single crystals: An electron-spin-resonance analysis, *Phys. Rev. B* **54**, 12353 (1996).
- [21] R. Ernst, S. Bodenhausen, and A. Wokaun, *Principles of NMR in One and Two Dimensions* (Oxford University Press, New York, 1987).
- [22] K. Koepnik and H. Eschrig, Full-potential nonorthogonal local-orbital minimum-basis band-structure scheme, *Phys. Rev. B* **59**, 1743 (1999); <http://www.FPLO.de>.
- [23] J. P. Perdew and Y. Wang, Accurate and simple analytic representation of the electron-gas correlation energy, *Phys. Rev. B* **45**, 13244 (1992).
- [24] J. P. Perdew, K. Burke, and M. Ernzerhof, Generalized Gradient Approximation Made Simple, *Phys. Rev. Lett.* **77**, 3865 (1996).
- [25] P. Blaha, K. Schwarz, F. Tran, R. Laskowski, G. K. H. Madsen, and L. D. Marks, WIEN2k: An APW+lo program for calculating the properties of solids, *J. Chem. Phys.* **152**, 074101 (2020).
- [26] R. Laskowski and P. Blaha, Calculating NMR chemical shifts using the augmented plane-wave method, *Phys. Rev. B* **89**, 014402 (2014).
- [27] D. J. Keeble, M. Loyo-Menoyo, Z. I. Y. Booq, R. R. Garipov, V. V. Eremkin, and V. Smotrakov, Fe³⁺ defect dipole centers in ferroelectric PbTiO₃ studied using electron paramagnetic resonance, *Phys. Rev. B* **80**, 014101 (2009).
- [28] D. J. Keeble, Z. Li, and E. H. Poindexter, Electron paramagnetic resonance of Mn⁴⁺ in PbTiO₃, *J. Phys.: Condens. Matter* **7**, 6327 (1995).
- [29] E. Erdem, R. Bottcher, H.-Ch. Semmelhack, H.-J. Glasel, and E. Hartmann, Multi-frequency EPR study of Cr³⁺ doped lead titanite (PbTiO₃) nanopowders, *Phys. Status Solidi B* **239**, R7 (2003).
- [30] W. Xiao-Xuan, Z. Wen-Chen, and F. Wang, Theoretical investigation of the EPR parameters for Cr³⁺ and Mn⁴⁺ ions in PbTiO₃ crystals, *Spectrochim. Acta A* **69**, 498 (2008).
- [31] A. Abragam and B. Bleaney, *Electron Paramagnetic Resonance of Transition Ions* (Clarendon Press, Oxford, 1970).
- [32] K. A. Muller, W. Berlinger, and J. Albers, Paramagnetic resonance and local position of Cr³⁺ in ferroelectric BaTiO₃, *Phys. Rev. B* **32**, 5837 (1985).
- [33] G. Volkel and K. A. Muller, Order-disorder phenomena in the low-temperature phase of BaTiO₃, *Phys. Rev. B* **76**, 094105 (2007).
- [34] E. Siegel and K. A. Muller, Local position of Fe³⁺ in ferroelectric BaTiO₃, *Phys. Rev. B* **20**, 3587 (1979).
- [35] A. Abragam, *Principles of Nuclear Magnetism* (Oxford University Press, New York, 1961).
- [36] J. F. Bangher, P. C. Taylor, T. Oja, and P. J. Bray, Nuclear magnetic resonance powder patterns in the presence of completely asymmetric quadrupole and chemical shift effects: Application to matavanadates, *J. Chem. Phys.* **50**, 4914 (1969).
- [37] T. J. Bastow, An NMR study of ¹³⁷Ba and ^{47,49}Ti in ferroelectric BaTiO₃, *J. Phys.: Condens. Matter* **1**, 4985 (1989).
- [38] D. Padro, A. P. Howes, M. E. Smith, and R. Dupree, Determination of titanium NMR parameters of ATiO₃ compounds: Correlations with structural distortion, *Solid State Nucl. Magn. Reson.* **15**, 231 (2000).
- [39] D. Padro, V. Jennings, M. E. Smith, R. Hoppe, P. A. Thomas, and R. Dupree, Variations of titanium interactions in solid state NMR—correlations to local structure, *J. Phys. Chem. B* **106**, 13176 (2002).
- [40] A. A. Koukoulas and M. A. Whitehead, Observations in nuclear quadrupole resonance frequency temperature dependence, *Chem. Phys. Lett.* **167**, 379 (1990).
- [41] A. García and D. Vanderbilt, First-principles study of stability and vibrational properties of tetragonal PbTiO₃, *Phys. Rev. B* **54**, 3817 (1996).
- [42] M. C. Kim, S. G. Lee, C. Joh, and H. S. Seo, First-principles predictions of structures and piezoelectric properties of PbTiO₃ single crystal, *Trans. Electr. Electron. Mater.* **17**, 29 (2016).
- [43] H. Mestric, R.-A. Eichel, T. Kloss, K.-P. Dinse, So. Laubach, St. Laubach, P. C. Schmidt, K. A. Schonau, M. Knapp, and H. Ehrenberg, Iron-oxygen vacancy defect centers in PbTiO₃: Newman superposition model analysis and density functional calculations, *Phys. Rev. B* **71**, 134109 (2005).
- [44] G. F. Reiter, W. Berlinger, K. Muller, and P. Heller, Paramagnetic-resonance studies of local fluctuations in SrTiO₃ above T_c, *Phys. Rev. B* **21**, 1 (1980).